High-Performance Flexible Organic Light-Emitting Diodes Using Embedded Silver Network Transparent Electrodes

Lei Zhou,[†] Heng-Yang Xiang,[†] Su Shen,[‡] Yan-Qing Li,[*,†] Jing-De Chen,[†] Hao-Jun Xie,[†] Irene A. Goldthorpe,[§] Lin-Sen Chen,[‡] Shuit-Tong Lee,[†] and Jian-Xin Tang[*,†]

[†]Institute of Functional Nano & Soft Materials (FUNSOM), Soochow University, Suzhou 215123, China, [‡]College of Physics Optoelectronics and Energy, Soochow University, Suzhou 215006, China, and [§]Department of Electrical and Computer Engineering, University of Waterloo, Waterloo, N2L 3G1, Canada

ABSTRACT Because of their mechanical flexibility, organic light-emitting diodes (OLEDs) hold great promise as a leading technology for display and lighting applications in wearable electronics. The development of flexible OLEDs requires high-quality transparent conductive electrodes with superior bendability and roll-to-roll manufacturing compatibility to replace indium tin oxide (ITO) anodes. Here, we present a flexible transparent conductor on plastic with embedded silver networks which is used to achieve flexible, highly power-efficient large-area green and white OLEDs. By combining an improved outcoupling structure for simultaneously extracting light in waveguide and substrate modes and reducing the surface plasmonic losses, flexible white OLEDs exhibit a power efficiency of 106 lm W^{-1} at 1000 cd m^{-2} with angular color stability, which is significantly higher than all other reports of flexible white OLEDs. These results represent an exciting step toward the realization of ITO-free, high-efficiency OLEDs for use in a wide variety of high-performance flexible applications.

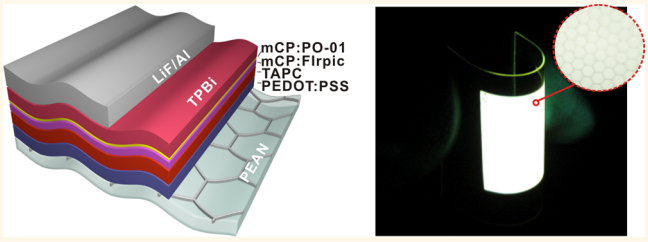

KEYWORDS: flexible OLEDs · flexible transparent conductor · superior bendability · silver networks

Mechanically flexible organic light-emitting diodes (OLEDs) are emerging as a leading technology for a variety of wearable intelligent electronics due to their unique capacity to be integrated with soft materials and curvilinear surfaces. Applications include bendable smartphones, foldable touch screens and antennas, paper-like displays, and curved and flexible solid-state lighting devices.[1−9] To date, the most commonly used transparent conductive electrode (TCE), indium−tin oxide (ITO), limits the further development of high-performance flexible OLED technology due to its inherent shortcomings such as brittleness, material scarcity, and a low-throughput deposition process.[10−12] It would be highly desirable to replace ITO with a new TCE solution which has low cost and improved bendability for future flexible, rollable, or foldable OLED-based applications.

Various types of flexible TCEs with attractive electrical and optical properties have been explored as alternative transparent conductors including graphene,[3,13−18] carbon nanotubes (CNTs),[19,20] Ag nanowires (NWs),[21,22] Cu NWs,[23,24] nanopatterned metallic films,[25,26] and conductive polymers.[27] Despite a strong potential to replace ITO, flexible OLEDs using these emerging TCEs show poorer efficiencies than ITO-based devices by a lack of efficient methods to improve charge injection and light outcoupling (Table S1, Supporting Information) and often are accompanied by complicated and hence unacceptably high-cost fabrication procedures. Further improvements on electrical and optical properties, chemical stability as well as the manufacturing process are required before they can be mass-produced as promising next-generation TCEs.

In addition to the aforementioned strategies, metallic grids, especially printed Ag grids,[28,29] have provided another route to improving the properties of TCEs.[30,31] Ag

* Address correspondence to jxtang@suda.edu.cn, yqli@suda.edu.cn.

Received for review October 22, 2014 and accepted December 3, 2014.

Published online December 03, 2014
10.1021/nn506034g

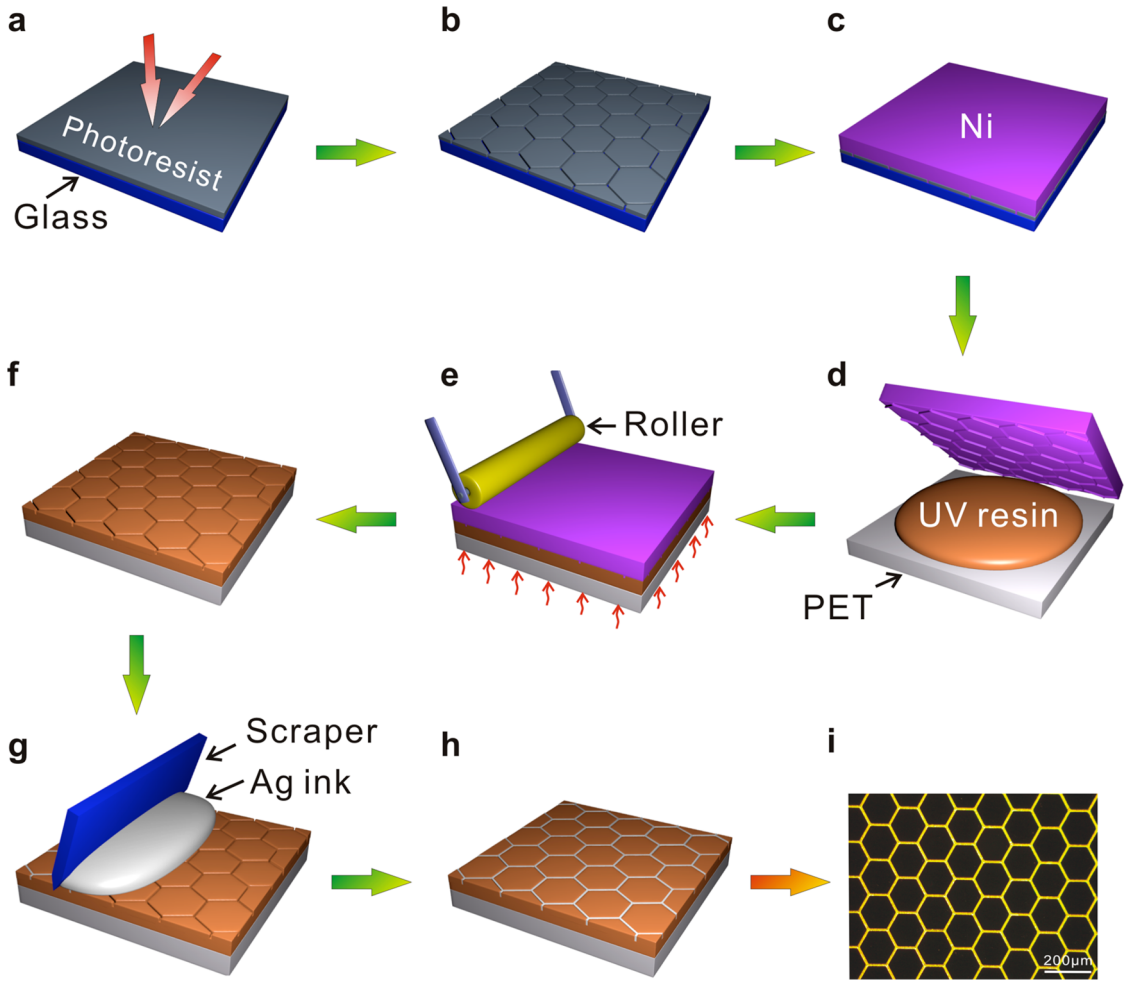

Figure 1. Schematic illustration of the fabrication steps of an embedded Ag network on PET substrate. (a) Fabrication of a hexagonal pattern on the photoresist on a glass substrate using photolithography. (b) Development of hexagonal photoresist mold. (c) Pattern transfer to a Ni mold using electroforming. (d) Dispersing UV resin on a PET substrate. (e) Mold transfer with UV nanoimprinting lithography. (f) Hexagonal pattern formation with plasma treating. (g) Dispersing the nanostructured Ag ink and scratching by Ag paste scratch technology. (h) Sintering and cleaning of the embedded Ag networks. (i) Dark-field microscopy image of Ag networks.

grids have been conventionally produced on the surface of the underlying substrate using approaches of inkjet printing,[32] direct ink writing,[33] and screen-printing.[34] However, these Ag grids used in organic devices may suffer electrical short-circuits and the loss of a conductive path due to the mismatch between the thickness of embossed metal grids (several micrometers) and the extremely thin organic layer (a few hundred nanometers).[35] Moreover, the poor adhesion of the grid to the substrate surface and the low throughput of roll-to-roll deposition with high resolution make existing Ag grids unsuitable for achieving highly efficient flexible OLEDs.[12]

Here we present a novel flexible TCE using plastic with embedded Ag networks (PEANs), whose fabrication process is time-saving and cost-effective with the combination of Ag paste scratch technology, nanoimprinting lithography, and precise pattern photolithography (Figure 1). The PEAN as a flexible TCE exhibits excellent optical, electrical, and mechanical properties, allowing little degradation of electrical properties upon bending. By employing an optimized light outcoupling structure with reduced ohmic losses, flexible green OLEDs yield a power efficiency (PE) > 120 lm W^{-1} and current efficiency (CE) >140 cd A^{-1} at a brightness of 1000 cd m^{-2}, while the flexible white OLEDs exhibit a maximum external quantum efficiency (EQE) of 49% and a record PE of 106 lm W^{-1} at 1000 cd m^{-2} with angular color stability. The performance of the flexible OLEDs using PEAN is competitive even to the best results reported from devices on ITO glass substrates,[15,36] which makes the present work promising for applications in large-area ITO-free flexible displays and lighting technologies.

RESULTS AND DISCUSSION

The fabrication process of PEANs is schematically described in Figure 1, which includes the nickel (Ni) mold design and fabrication, pattern transfer to a film of UV resin coated on polyethylene terephthalate

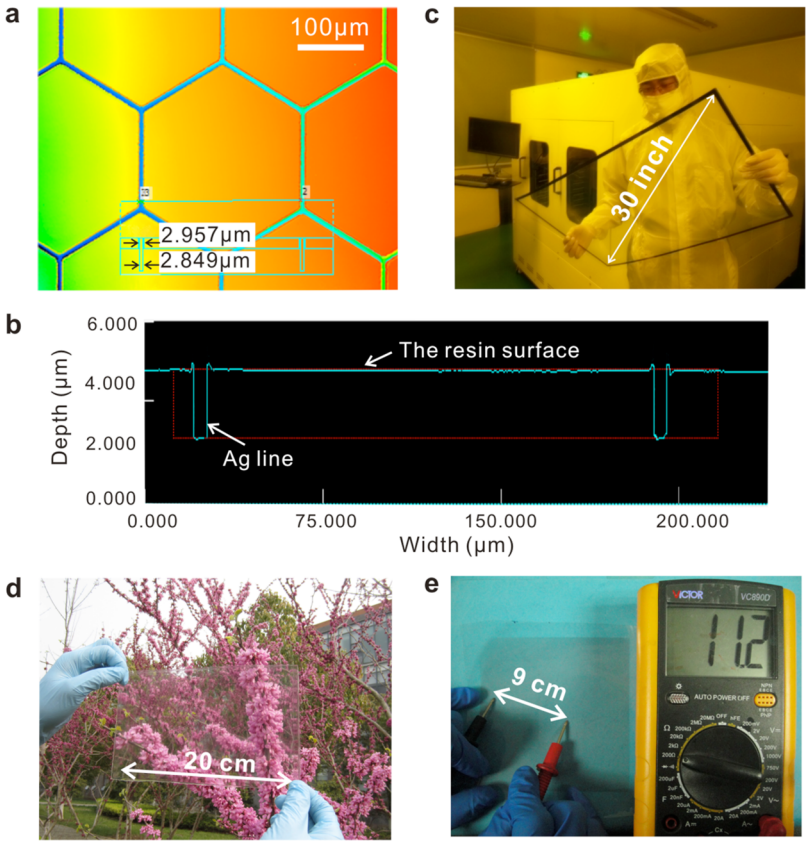

Figure 2. Experimental realization of PET with embedded Ag networks (PEANs) as a transparent conductive electrode. (a, b) The three-dimensional confocal microscopy images of the top-view (a) and depth profile (b) of the hexagonal Ag networks (period of 150 μm, groove depth of ~3 μm, and width of ~3 μm). (c) Optical image of the PEAN substrate with a diagonal size of 30 in. (d) Close view of a PEAN under ambient conditions. (e) Electrical resistance testing of the PEAN using an ohmmeter.

(PET) substrates by imprinting, the filling of conductive nanostructured Ag ink into the embedded groove structure by scraping, and finally sintering. First, an embedded hexagonal groove structure of various periodicities was transferred to the photoresist (RZJ-390PG, Ruihong Electronic Chemical Co., Ltd.) on a glass substrate after exposure by digital micromirror devices (DMD)-based photolithography (iGrapher200, SVG DigitOptics, Co., Ltd.). The network structures can be easily tuned and obtained by adjusting the patterns on the DMD transferred by the computer. Upon development in NaOH (0.4%) solution for 4 s and subsequent drying in air, the hexagonal groove structure was transferred to a Ni mold through electroforming. For the pattern transfer, a 10 μm thick UV-curable resin (D10, PhiChem), which was drop-dispensed on PET film, was imprinted by the Ni stamp with a pressure of 3.0 bar for 30 s under UV irradiation. For this purpose, an in-house built roll-to-plane UV nanoimprinting lithography system was used at an intensity of 1000 mW cm^{-2} (SVG DigitOptics, Co., Ltd.). After the Ni stamp was peeled from the patterned UV resin, the surface of the UV-curable resin film was plasma-treated to improve its hydrophilic property. Conductive nanostructured Ag ink (particle diameter between 2 and 10 nm, concentration of 41%, viscosity of 55 cps and surface tension of 30 dyn cm^{-1}) was sequentially drop-dispensed on the patterned UV film to fill the hexagonal trenches, and the excess Ag was removed by means of scraping. Meanwhile, to make the surface clear, the wiping process was performed with nontoxic organic solvents (*e.g.*, ethanol). Finally, the flexible PEAN was sintered at 100 °C for 6 min in the infrared-assisted oven. Notably, the fabrication of PEANs is free from expensive vacuum techniques and is entirely solution-processed at a low temperature, which is compatible with plastic substrates and low-cost roll-to-roll manufacturing.

Figure 2a presents a representative image of a hexagonal Ag network with a 150 μm period, ~2 μm groove depth, and ~3 μm groove width. The period of the Ag networks are several orders of magnitude larger than the visible wavelength, which minimizes light diffraction. The PEANs exhibit highly optical transmittance (Figure 2d) and electrical conductivity (Figure 2e), which can be tuned by tailoring the period of the hexagonal array (Figures S1 and S2, Supporting Information). The PEANs with a period of 150 μm possess a transmittance >87% in the wavelength range of 400−800 nm (Figure S1, Supporting Information) and a sheet resistance <5 Ω □$^{-1}$ (Figure S2, Supporting Information), which is superior to the performance of reported TCEs in the scientific literature, such as Ag

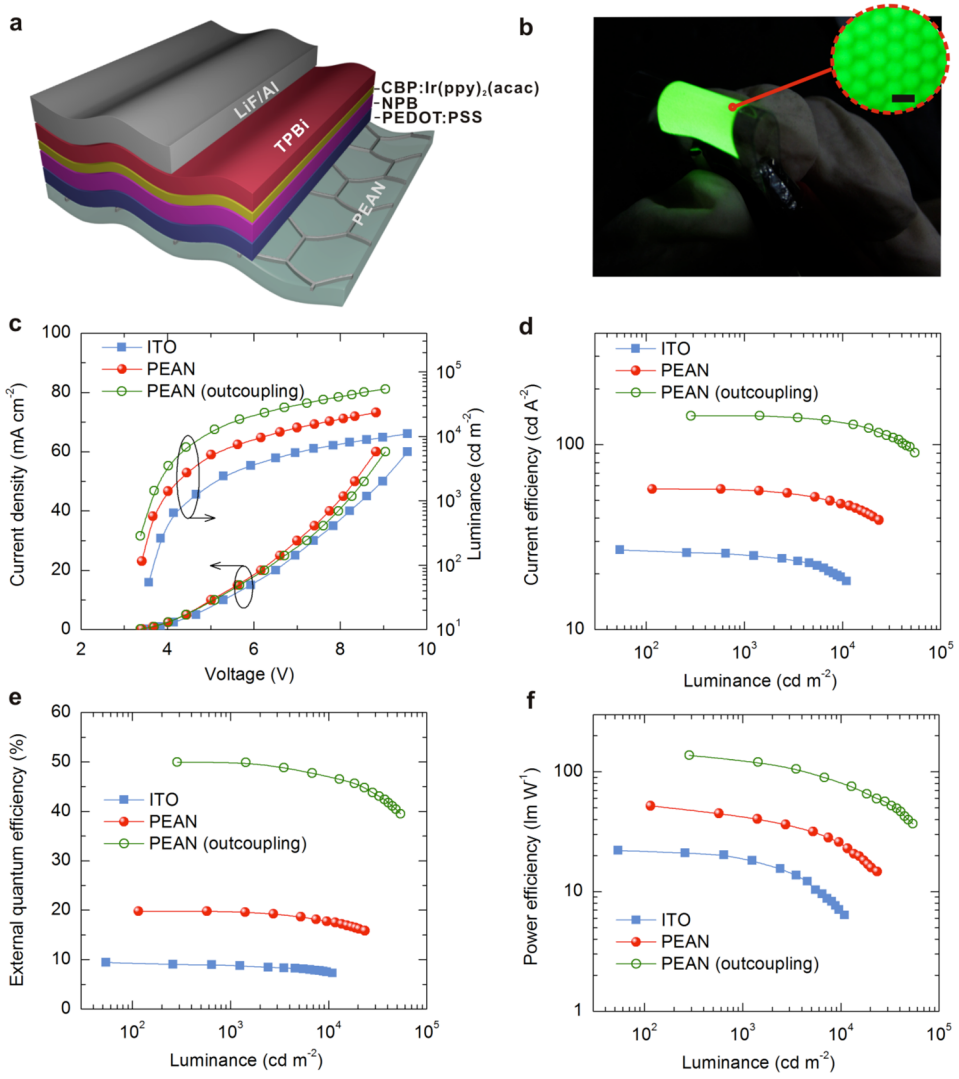

Figure 3. Device structure and performance of flexible green OLEDs. (a) Schematic illustration of flexible green OLEDs using PEAN as the anode. (b) Optical image of light emission from a flexible green OLED (12 mm × 12 mm) using a PEAN anode. Inset: the magnified image using an optical microscope (scale bar = 300 μm). (c) Current density and luminance as a function of driving voltage of flexible green OLEDs using PEANs (without and with an outcoupling structure) or ITO−PET as the anode. (d−f) Current efficiencies (d), external quantum efficiencies (e), and power efficiencies (f) of flexible green OLEDs as a function of luminance.

NWs,[37] CNTs,[20] metal grids,[38] and ITO[39,40] (Figure S2, Supporting Information). In addition to the total transmittance properties, the amount of light scattering present in PEANs is determined by measuring the specular and diffuse transmission. The transmittance haze represents the percentage of light diffusely scattered compared to the total light transmitted, which is one of the pivotal features in display applications.[41,42] The haze values of PEANs are strongly dependent on the period of the Ag networks. A PEAN with a 150 μm period exhibits an average haze value of ~4.3% over the visible spectrum, which is comparable to that of ITO-coated PET (ITO−PET, haze ≈ 4.9%) and bare PET substrates (haze ≈ 4.3%) (Figure S3, Supporting Information). Such low haze indicates that the PEAN would maintain transparency without causing additional optical modes (an optical image of the PEAN is shown in Figure 2b), which is a requisite of high-resolution displays.[42] Moreover, the PEAN can keep sufficient scratch resistance since the Ag networks are filled in the grooves of the UV resin (Figure S4, Supporting Information).

Phosphorescent green OLEDs were fabricated on both flexible PEANs and ITO−PET substrates for comparison, as schematically shown in Figure 3a (also see Figure S5, Supporting Information). An 80 nm thick conductive layer of PEDOT:PSS was spin-coated on the electrode surface as a hole injection layer, which enables holes to be injected efficiently into the overlying organic emissive layer (EML). Moreover, the PEDOT:PSS layer is favorable for smoothing the surface roughness of the PEAN and ITO−PET substrates (Figure S6, Supporting Information). It is clearly noted from the AFM measurements that the roughness of the

TABLE 1. Performance Characteristics for Flexible OLEDs (size: 12 mm × 12 mm)[a]

	device structures	CE (1000 cd m^{-2}) (cd A^{-1})	EQE (1000 cd m^{-2}) (%)	PE (1000 cd m^{-2}) (lm W^{-1})	EQE (max) (%)	PE (max) (lm W^{-1})
green	ITO	25.3	8.8	18.8	9.4	25.2
	PEAN	57.2	19.6	42.3	19.8	52.0
	PEAN (outcoupling)	143.1	49.9	123.5	50.0	137.5
white	ITO	22.6	8.2	16.1	9.1	19.1
	PEAN	48.5	17.8	42.6	18.5	49.4
	PEAN (outcoupling)	121.5	46.3	106.0	49.0	118.1

[a] The CE, PE, and EQE values are compared at their maximum values and at a luminance of 1000 cd m^{-2}.

PEDOT:PSS layer on the ITO−PET substrate is ~3.2 nm, while it remains ~8.7 nm for the case of PEAN substrate. It indicates that the surface roughness of the PEANs can be significantly reduced with an 80 nm thick PEDOT:PSS coating for the fabrication of OLEDs. The organic EML was composed of a 45 nm thick hole-transporting layer (HTL) of *N*,*N*′-di(naphthalen-1-yl)-*N*,*N*′-diphenylbenzidine (NPB), a 20 nm thick layer of 4,4′-bis(carbazol-9-yl)biphenyl (CBP) doped with 7 wt % bis(2-phenylpyridine)(acetylacetonate)iridium(III) [$Ir(ppy)_2(acac)$] for green emission,[43] and a 40 nm thick electron-transporting layer (ETL) of 2,2′,2″-(1,3,5-benzinetriyl)tris(1-phenyl-1*H* -benzimidazole) (TPBi). A LiF (1 nm)/Al (100 nm) bilayer was used as the cathode. The photograph of green OLEDs using PEAN shows uniform light emission (Figure 3b). Furthermore, the embedded Ag networks can only be detected by microscopy with magnification and thus do not affect the quality of display and lighting for viewing.

The current density−voltage (I−V) characteristics in Figure 3c show that green OLEDs using PEAN possess a slightly reduced driving voltage than the device on ITO−PET. The comparison of the sheet resistances of PEAN (~4.7 Ω □$^{-1}$) and ITO−PET (20 Ω □$^{-1}$), both of which have similar transparency, indicates that the improved electrical properties for devices using PEAN is due to lower electrode series resistance. More importantly, the luminance−voltage characteristics (Figure 3c) show that the luminance at a constant driving voltage of OLEDs using PEAN is significantly enhanced in comparison to the case of ITO−PET. As can be seen in Figure 3d−f, the use of PEANs in flexible green OLEDs yields a CE of 57.2 cd A^{-1}, an EQE of 19.6%, and a PE of 42.3 lm W^{-1} at a luminance of 1000 cd m^{-2}, which is over 2 times larger than that using ITO−PET (the detailed device characteristics are summarized in Table 1). In adition, only a small efficiency roll-off at high luminance can be observed for OLEDs using PEANs as compared to that with ITO−PET substrates. For example, the efficiency decreases for CE and EQE in devices using PEANs are 16.4% and 9.7%, respectively, when the luminance is increased from 1,000 cd m^{-2} to 10,000 cd m^{-2}. In contrast, the corresponding values in ITO−PET based devices are 29.2% and 19.3% for CE and EQE, respectively (Table S2, Supporting Information). It indicates the excellent charge injection from the Ag network to the organic layers for balanced charge transport and efficient exciton generation. In addition, the performance of the flexible green OLED using PEAN is comparable with the device using ITO on glass substrate with the same emission area of 14 mm × 14 mm (Figure S7, Supporting Information), demonstrating the promise of PEANs as an alternative TCE to replace ITO in large-area OLEDs.

To characterize the optical effect of PEANs on actual emission behaviors, we perform optical modeling calculations (see the Methods for details of the optical modeling). The relative EQE intensities simulated with the Monte Carlo ray tracing method indicate that the enhancement ratio of OLEDs using PEAN in comparison with that on ITO−PET could be as high as ~2.64 (Figure S8, Supporting Information), which is comparable with the experimental value (for example, ~2.1 for devices without an outcoupling structure in Figure 3). The slight discrepancy between the optical model and experimental results might originate from the difference in the refractive indices of the ITO layer, the emission layer, and the plastic substrate. To further understand the EQE enhancement, the distributions of the electric field intensities for one transverse-electric (TE_0) and two transverse-magnetic (TM_0 and TM_1) waveguide modes were calculated for flexible green OLEDs on PEAN and ITO−PET using the FDTD method. For the device on ITO−PET, the maximum electric field intensity of the TE_0 mode is located in the ITO layer, and a large part of the TM_0 and TM_1 modes also lie in the ITO layer (Figure S9a, Supporting Information). On the contrary, replacing the ITO electrode with a PEAN leads to a substantial suppression of waveguide modes (*e.g.*, TE_0, TM_0, and TM_1 modes originally trapped within the ITO layer), and thus a significant gain of substrate modes (Figure S9b, Supporting Information). The variation of the electric field distributions in flexible OLEDs on PEAN and ITO−PET is due to the well refractive-index matching of PEAN (n = 1.49) to PEDOT:PSS (1.46) and typical organic layers (n = 1.75) rather than that using ITO (n = 1.85).[44] The removal of the high refractive-index ITO layer results in the dramatic elimination of the amount of photon flux trapped in the ITO/organic waveguide mode, and thus the enhancement in coupling of the emitted light from the organic EML into the

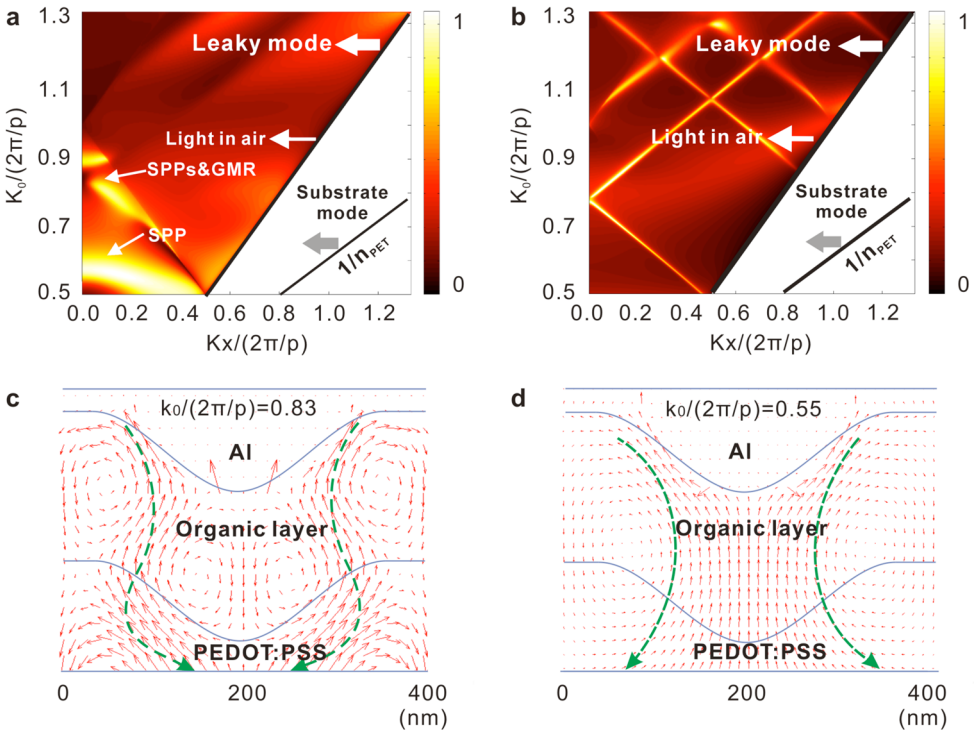

Figure 4. Simulation of an OLED device using a PEAN with an outcoupling structure. (a, b) Calculated dispersion diagrams of TM (a) and TE (b) polarized light as a function of frequency and the in-plane wave vector Kx in the first Brillouin zone of the device with an outcoupling structure. (c, d) Photon flux diagrams of the poynting vector S distribution at $k_0/(2\pi/p) = 0.83$ (c) and $k_0/(2\pi/p) = 0.55$ (d). Red arrows depict the flow direction of the photon flux, and the green dash arrows illustrate the main direction of liberating the photon flux trapped within an OLED with an outcoupling structure. A thicker and longer arrow tail indicates a stronger intensity of the photon flux.

substrate. Correspondingly, the higher light outcoupling efficiency and the EQE enhancement are expected for OLEDs using PEAN in comparison with the device on ITO, which are consistent with the results of experimental device characteristics (Figure 3).

The flexibilities of OLEDs using PEAN and ITO–PET were tested by repeatedly bending the substrates to a radius of curvature of about 6 mm at a constant current density of 15 mA cm^{-2}. The flexible OLEDs using PEAN show stable operation under repeated bends with only a small decrease in efficiency, less than ~19% after 1,000 bending cycles. The device on ITO–PET on the other hand exhibits a quick degradation to failure upon the same repeated bending due to cracking in the brittle ITO and the decrease in conductivity (Figure S10, Supporting Information), which demonstrates the superior bending stability of PEAN compared to ITO.

It is known that light outcoupling efficiency is limited in conventional OLED structures without a light extraction scheme because 70–80% of the emitted light is confined in the substrate and waveguide modes, or lost by the surface plasmon polariton of the metal electrode (SPP mode).[45] To further enhance luminance and efficiency, a light outcoupling structure for liberating the trapped photons was integrated into the flexible devices by nanoimprinting the PEDOT:PSS layer with deterministic aperiodic nanostructures (DANs) and applying a microlens array (MLA) to the plastic substrate (Figures S11 and S12, Supporting Information).[46–48] It is evident in Figure 3c that OLEDs with and without the light outcoupling structure have nearly identical current–voltage characteristics, indicating that the patterning of the PEDOT:PSS layer has negligible influence on the contact resistance and charge injection behavior. However, the luminance and efficiency of the device with an outcoupling structure (Figure 3d–f) are dramatically increased with a CE of 143.1 cd A^{-1}, an EQE of 49.9%, and a PE of 123.5 lm W^{-1} at 1000 cd m^{-2}, respectively. Note that the outcoupling enhancement of light is the combined effect of the DANs and the MLA (Figure S13, Supporting Information), where the DANs promote the extraction of light originally trapped in the organic waveguide mode into the plastic substrate[49] and the MLA extracts light from the substrate to the air.[48] The resulting PE at a luminance of 1,000 cd m^{-2} is ~2.9 times that of the OLED using PEAN without outcoupling.

To elucidate the optical enhancement mechanisms of flexible OLEDs using PEAN with an outcoupling structure, an electromagnetic analysis based on RCWA method was employed to solve Maxwell's equations in two dimensions. Figure 4a,b presents the calculated dispersion diagrams of TM and TE polarized lights as a function of frequency and in-plane wave vector **Kx** in the first Brillouin zone of the device with an outcoupling structure of the DANs. According to the

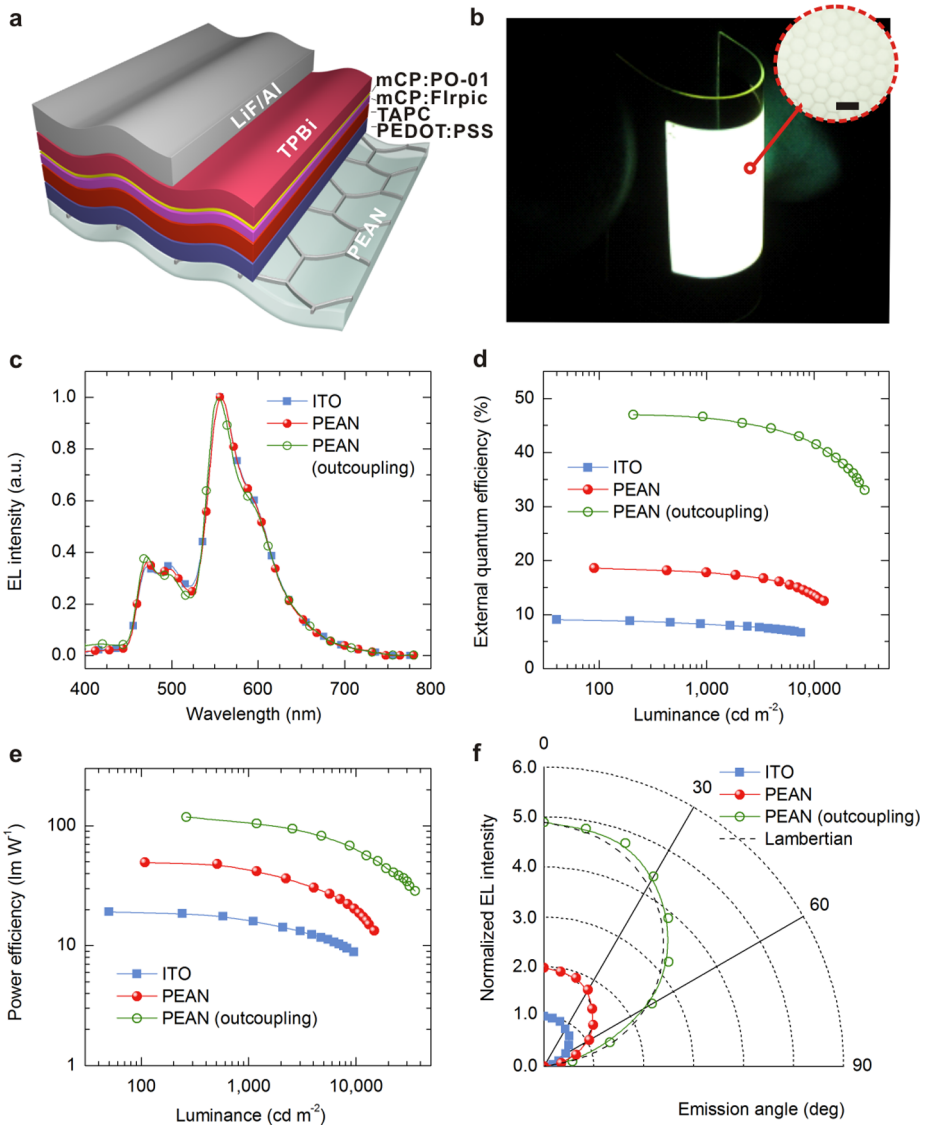

Figure 5. Device structure and performance of flexible white OLEDs. (a) Schematic of flexible white OLED device structure using PEAN as anode. (b) Photograph of a large-area flexible white OLED (50 mm × 50 mm) using PEAN as anode. Inset: the magnified image taken with an optical microscope (scale bar = 3.00 μm). (c) Electroluminescence spectra of flexible white OLEDs using PEAN (without and with an outcoupling structure) or ITO−PET as anode at a current density of 15 mA cm^{-2}. (d, e) External quantum efficiencies (d) and power efficiencies (e) as a function of luminance for flexible white OLEDs. (f) Angular dependence of light intensity for flexible white OLED devices. The dashed line represents the ideal Lambertian emission pattern.

previous reports,[50−52] the enhanced out-coupling and the extraordinary optical absorption in the nanostructured OLEDs can be attributed to the same resonant optical mode in the structure. The phenomenon of light coupling by waveguide modes is clearly observed with a comprehensive optical response occurring for TM polarization (Figure 4a).[53] Compared to the device without an outcoupling structure (Figure S14, Supporting Information), the use of DANs allows efficient photon flux transfer from a guided-mode resonance (GMR) to leaky modes ($K_X/(2\pi/P) < K_0$) for both TM (Figure 4a) and TE (Figure 4b) polarized light. Strongly damped SPP modes can be excited as a consequence of the corrugated metal electrode induced by the incorporation of the DANs, which split into two branches due to Rayleigh-Wood anomalies.[54] It can be observed in the photon flux diagrams of the pointing vector **S** (Figure 4c) that at a specific resonant frequency $k_0/(2\pi/p) = 0.83$ a hybrid interaction between the SPP (at a resonant frequency of $k_0/(2\pi/p) = 0.55$, Figure 4d) and the GMR enables the photon flux propagation as an extraordinary optical vortex. With this fantastic complex coupling, the trapped energy power within the ordinary flat OLEDs could be more efficiently extracted.

The device structure of a phosphorescent white OLED using PEAN is depicted in Figure 5a. *N*,*N*′-Dicarbazolyl-3,5-benzene (mCP) was selected as the host material due to its high triplet energy, and a 45 nm thick di[4-(*N*,*N*-ditolylamino)phenyl]cyclohexane

(TAPC) was employed as the HTL to match the deep highest occupied molecular orbital level of mCP. The white EML with two complementary colors used a 19 nm thick mCP layer doped with 8 wt % bis(3,5-difluoro-2-(2-pyridyl)phenyl-(2-carboxypyridyl)iridium-(III) (FIrpic) for blue emission and a 1 nm thick mCP layer doped with 6 wt % iridium(III) bis(4-phenylthieno[3,2-*c*]pyridinato-N,C2′) acetylacetonate (PO-01) for yellow emission. A 40 nm thick TPBi was used as the ETL, which was followed by a LiF (1 nm)/Al (100 nm) bilayer cathode. The picture of a large-area flexible white OLED (50 mm × 50 mm) using PEAN shows that the uniform white light is emitted and an illuminated object exhibits vivid color (Figure 5b), indicating the capability for general lighting. The emission spectra of flexible OLEDs on PEAN and ITO−PET are almost identical to each other with the use of the outcoupling structure (Figure 5c), indicating no grating effects and a wavelength-independent response. The flexible white OLEDs have Commission Internationale d'Eclairage coordinates of (0.397, 0.478), (0.398, 0.477), and (0.396, 0.460) for the device structures using ITO−PET, PEAN, and PEAN with an outcoupling structure, respectively.

The EQE and PE of white OLEDs on PEAN and ITO−PET are plotted as a function of luminance in Figure 5d,e. Flexible white OLEDs using PEAN yield a CE of 48.5 cd A^{-1}, an EQE of 17.8%, and a PE of 42.6 lm W^{-1} at 1000 cd m^{-2}, which is over 2 times that on ITO−PET (CE = 22.6 cd A^{-1}, EQE = 8.2%, and PE = 16.1 lm W^{-1}) (Table 1). The use of the light-outcoupling structure including DANs and MLA can further increase the light extraction and thus the device efficiency without spectral distortion (Figure S15, Supporting Information). The maximum EQE and PE of flexible white OLEDs using PEAN are recorded as 49% and 118.1 lm W^{-1}. Moreover, the flexible device still maintains EQE = 46.3% and PE = 106 lm W^{-1} at 1000 cd m^{-2}, which are much higher than previous reports of flexible white OLEDs in the scientific literature and even competitive to white OLEDs on glass substrates (Table S1, Supporting Information).

The angular dependence of light intensity is displayed in Figure 5f. It is also interesting to note that flexible white OLEDs using PEANs with and without the outcoupling structure both show a Lambertian emission pattern with a maximum intensity in the normal direction, which is consistent with the device on ITO−PET. Additionally, the emission for OLEDs using PEAN with and without the outcoupling structure keeps a nearly identical spectral shape with increasing viewing angle, resulting in an angular-independent white emission (Figure S16, Supporting Information). The angular independence of color stability in the device with an outcoupling structure is due to the excellent capability of quasi-omnidirectional light extraction of the DANs and the MLA for use in full-color OLEDs.[46] Correspondingly, the color stability with viewing angle in flexible white OLEDs using PEAN would be beneficial to high-quality white lighting applications.

CONCLUSIONS

In conclusion, we have demonstrated an innovative flexible TCE based on PEANs with high optical transparency, high conductivity, and good bending capability. The PEANs have a lower sheet resistance in comparison with ITO at a given transparency, which is beneficial to the realization of large-area organic devices without substantial efficiency losses. The low surface roughness of PEANs is favorable for the subsequent deposition of organic layers without suffering electrical short circuits. By combining an optimized outcoupling structure, the large-area ITO-free flexible white OLEDs show a record performance among all OLEDs using flexible TCEs, yielding a maximum PE > 115 lm W^{-1} with an ideal Lambertian emission pattern and superior angular color stability. A table comparing the performance of our OLEDs to other OLEDs reported in the literature is displayed in Table S1 (Supporting Information). The flexible device presented in this work has the potential to achieve an even higher efficiency if all the device parameters and optical structures are continuously optimized to reduce the energetic and outcoupling losses during electron-photon conversion. The approach demonstrated here opens up the opportunity to other large-scale roll-to-roll fabrication technologies for wearable optoelectronics with high performance and low manufacturing and materials cost.

METHODS

Device Fabrication. The glass and PET substrates coated with ITO electrodes were cleaned with detergent, ethanol, and DI water for 20 min each and dried in an oven. The PEANs were cleaned with ethanol and dried in an oven. The 80 nm thick poly(3,4-ethylenedioxythiophene):poly(styrenesulfonate) (PEDOT:PSS, with 5 vol % dimethy1 sulfoxide and mixed with 0.5 vol % Zonyl FS-300 fluorosurfactant from Fluka to promote wetting on the UV-curable resin) was spin-coated onto PEANs and ultraviolet-ozone (UVO) treated ITO substrates in ambient conditions, followed by a 120 °C bake on a hot plate for 20 min before the subsequent organic deposition. To prepare the deterministic aperiodic nanostructures (DANs) on the PEDOT:PSS layer, a vacuum-assisted thermal nanoimprinting method was introduced with a flexible perfluoropolyether (PFPE) mold on the basis of soft nanoimprint lithography. The preliminary nanopatterned PEDOT:PSS samples were annealed at 140 °C under atmospheric conditions for a further 10 min to consummate the high-profile three-dimensional subwavelength patterns and maintain the highly efficient electrical properties. The imprinting recipe was optimized by a systematic study of the imprinting time and pressure. The substrates with the PEDOT:PSS layer were transferred into a high-vacuum chamber with base pressure of <5 × 10^{-7} Torr for film

deposition by thermal evaporation with a shadow mask. The deposition rate and film thickness were monitored by a quartz crystal oscillator. The emission areas of devices are 144 mm^2 on PEANs and 10 mm^2 on ITO–PET, respectively. The devices on ITO-glass, ITO–PET, and PEAN without and with an outcoupling structure were fabricated at the same time to ensure consistent results.

Device Characterization. The current density–voltage–luminance (J–V–L) characteristics and electroluminescence spectra of the corresponding devices were measured simultaneously in ambient air using a computer-controlled programmable Keithley model 2400 power source and a PhotoResearch PR655 luminance meter/spectrometer. The angle-dependent emission intensity was characterized by placing the devices on a rotating stage with one of the grooves parallel to the rotation axis. The refractive index (n), extinction coefficient (k), and film thickness of all the films were measured using the alpha-SE Spectroscopic Ellipsometer (J.A.Woollam Co., Inc.). Optical transmission spectra were recorded by a UV/vis/near-IR spectrophotometer (PerkinElmer Lambda 750) with an integrating sphere. Surface morphologies were characterized by atomic force microscopy (AFM) (Veeco MultiMode V) in tapping mode and scanning electron microscopy (SEM) (FEI, Quanta 200FEG). The sheet resistances of all TCEs were measured using a digital multimeter (Keithley 2100) with a four-point probe configuration to eliminate contact resistance.

Theoretical Modeling. The in-plane waveguide modes for TE and TM polarized light in OLEDs were simulated based on the finite difference time domain (FDTD) approach (Lumerical FDTD Solutions 8.7.3). In order to find a solution to identify the variation of effective refractive index of the OLED devices, the three-dimensional Monte Carlo ray tracing method was adopted by assuming a Lambertian point source (1 W, 20000 rays) located within the sample substrate (10 × 10 × 0.8 mm) and the Al cathode film as a perfect reflector. For devices with nanostructured patterning, geometric optics based on the ray tracing method cannot be used for simulating the photon flux distribution in nanoscale optical fields. To find a rigorous solution to Maxwell's equations in the device with an outcoupling structure of DANs, rigorous coupled wave analysis (RCWA) was adopted to model the dispersion diagram (Rsoft DiffractMOD and corresponding codes generated in-house), and the FDTD method was used to simulate the poynting vector **S** distribution (Rsoft Fullwave) with commercial RSoft 8.1 (RSoft Design Group, Inc.). The complex optical dielectric function of the nanostructured Al cathode was fitted using the Drude–Lorentz model, taking into account interband transitions and the frequency-dependent refractive index (n) and extinction coefficient (k) of PEDOT:PSS, ITO, and PET experimentally determined by the ellipsometer.

Conflict of Interest: The authors declare no competing financial interest.

Acknowledgment. We acknowledge financial support from the National Basic Research Program of China (Grant No. 2014CB932600), the National Natural Science Foundation of China (Grant Nos. 91433116, 91323303, 11474214, 61107022), Jiangsu Science and Technology Department (No. BK20140053), Natural Science Foundation of the Higher Education Institutions of Jiangsu Province (Grant No. 10KJA140048), Collaborative Innovation Center of Suzhou Nano Science and Technology, Jiangsu Key Laboratory for Carbon-Based Functional Materials & Devices, and the project of the Priority Academic Program Development (PAPD) of Jiangsu Higher Education Institutions.

Supporting Information Available: Basic information about the comparison of flexible OLEDs reported in the literature, the fabrication process of PEANs, and the corresponding characterization of their optical, morphological, and electrical properties, the simulation of light extraction, the bending stability of flexible OLEDs, and the device performance of flexible devices with PEANs with an outcoupling structure are also presented. This material is available free of charge *via* the Internet at http://pubs.acs.org.

REFERENCES AND NOTES

1. Ramuz, M.; Tee, B. C-K.; Tok, J. B.-H.; Bao, Z. Transparent, Optical, Pressure-Sensitive Artificial Akin for Large-Area Stretchable Electronics. *Adv. Mater.* **2012**, *24*, 3223–3227.
2. Jung, S.; Lee, S.; Song, M.; Kim, D. G.; You, D. S.; Kim, J. K.; Kim, C. S.; Kim, T. M.; Kim, K. H.; Kim, J. J.; et al. Extremely Flexible Transparent Conducting Electrodes for Organic Devices. *Adv. Energy. Mater.* **2014**, *4*, 1–8.
3. Han, T.-H.; Lee, Y.; Choi, M.-R.; Woo, S.-H.; Bae, S.-H.; Hong, B. H.; Ahn, J.-H.; Lee, T.-W. Extremely Efficient Flexible Organic Light-Emitting Diodes with Modified Graphene Anode. *Nat. Photonics* **2012**, *6*, 105–110.
4. Sekitani, T.; Someya, T. Stretchable, Large-Area Organic Electronics. *Adv. Mater.* **2010**, *22*, 2228–2246.
5. Liang, J.; Li, L.; Niu, X.; Yu, Z.; Pei, Q. Elastomeric Polymer Light-Emitting Devices and Displays. *Nat. Photonics* **2013**, *7*, 817–824.
6. Rogers, J. A.; Someya, T.; Huang, Y. Materials and Mechanics for Stretchable Electronics. *Science* **2010**, *327*, 1603–1607.
7. Sekitani, T.; Nakajima, H.; Maeda, H.; Fukushima, T.; Aida, T.; Hata, K.; Someya, T. Stretchable Active-Matrix Organic Light-Emitting Diode Display Using Printable Elastic Conductors. *Nat. Mater.* **2009**, *8*, 494–499.
8. Kim, R. H.; Bae, M. H.; Kim, D. G.; Cheng, H.; Kim, B. H.; Kim, D. H.; Li, M.; Wu, J.; Du, F.; Kim, H. S.; *et al.* Stretchable, Transparent Graphene Interconnects for Arrays of Microscale Inorganic Light Emitting Diodes on Rubber Substrates. *Nano Lett.* **2011**, *11*, 3881–3886.
9. Sandström, A.; Dam, H. F.; Krebs, F. C.; Edman, L. Ambient Fabrication of Flexible and Large-Area Organic Light-Emitting Devices Using Slot-Die Coating. *Nat. Commun.* **2012**, *3*, 1002.
10. Cai, M.; Ye, Z.; Xiao, T.; Liu, R.; Chen, Y.; Mayer, R. W.; Biswas, R.; Ho, K. M.; Shinar, R.; Shinar, J. Extremely Efficient Indium-Tin-Oxide-Free Green Phosphorescent Organic Light-Emitting Diodes. *Adv. Mater.* **2012**, *24*, 4337–4342.
11. Peng, C.; Jia, Z.; Neilson, H.; Li, T.; Lou, J. *In Situ* Electro-Mechanical Experiments and Mechanics Modeling of Fracture in Indium Tin Oxide-Based Multilayer Electrodes. *Adv. Energy Mater.* **2013**, *15*, 250–256.
12. Ellmer, K. Past Achievements and Future Challenges in the Development of Optically Transparent Electrodes. *Nat. Photonics* **2012**, *6*, 809–817.
13. Kasry, A.; Kuroda, M. A.; Martyna, G. J.; Tulevski, G. S.; Bol, A. A. Chemical Doping of Large-Area Stacked Graphene Films for Use as Transparent Conducting Electrodes. *ACS Nano* **2010**, *4*, 3839–3844.
14. Huang, X.; Zeng, Z.; Fan, Z.; Liu, J.; Zhang, H. Graphene-Based Electrodes. *Adv. Mater.* **2012**, *24*, 5979–6004.
15. Li, N.; Oida, S.; Tulevski, G. S.; Han, S. J.; Hannon, J. B.; Sadana, D. K.; Chen, T. C. Efficient and Bright Organic Light-Emitting Diodes on Single-Layer Graphene Electrodes. *Nat. Commun.* **2013**, *4*, 2294.
16. Wu, J.; Agrawal, M.; Becerril, H. A.; Bao, Z.; Liu, Z. F.; Chen, Y. S.; Peumans, P. Organic Light-Emitting Diodes on Solution-Processed Graphene Transparent Electrodes. *ACS Nano* **2010**, *4*, 43–48.
17. Kim, K. S.; Zhao, Y.; Jang, H.; Lee, S. Y.; Kim, J. M.; Kim, K. S.; Ahn, J. H.; Kim, P.; Choi, J. Y.; Hong, B. H. Large-Scale Pattern Growth of Graphene Films for Stretchable Transparent Electrodes. *Nature* **2009**, *457*, 706–710.
18. Bae, S.; Kim, H.; Lee, Y. B.; Xu, X. F.; Park, J. S.; Zheng, Y.; Balakrishnan, J.; Lei, T.; Kim, H. R.; Song, Y. I.; *et al.* Roll-to-Roll Production of 30-Inch Graphene Films for Transparent Electrodes. *Nat. Nanotechnol.* **2010**, *5*, 574–578.
19. Hecht, D. S.; Hu, L. B.; Irvin, G. Emerging Transparent Electrodes Based on Thin Films of Carbon Nanotubes, Graphene, and Metallic Nanostructures. *Adv. Mater.* **2011**, *23*, 1482–1513.
20. Geng, H. Z.; Kim, K. K.; So, K. P.; Lee, Y. S.; Chang, Y.; Lee, Y. H. Effect of Acid Treatment on Carbon Nanotube-Based Flexible Transparent Conducting Films. *J. Am. Chem. Soc.* **2007**, *129*, 7758–7759.

21. Hu, L.; Kim, H. S.; Lee, J. Y.; Peumans, P.; Cui, Y. Scalable Coating and Properties of Transparent, Flexible, Silver Nanowire Electrodes. *ACS Nano* **2010**, *4*, 2955–2963.
22. Gaynor, W.; Hofmann, S.; Christoforo, M. G.; Sachse, C.; Mehra, S.; Salleo, A.; McGehee, M. D.; Gather, M. C.; Lüssem, B.; Müller-Meskamp, L.; *et al.* Color in the Corners: ITO-Free White OLEDs with Angular Color Stability. *Adv. Mater.* **2013**, *25*, 4006–4013.
23. Wu, H.; Hu, L. B.; Rowell, M. W.; Kong, D.; Cha, J. J.; McDonough, J. R.; Zhu, J.; Yang, Y.; McGehee, M. D.; Cui, Y. Electrospun Metal Nanofiber Webs as High-Performance Transparent Electrode. *Nano Lett.* **2010**, *10*, 4242–4248.
24. Rathmell, A. R.; Bergin, S. M.; Hua, Y. L.; Li, Z. Y.; Wiley, B. J. The Growth Mechanism of Copper Nanowires and Their Properties in Flexible, Transparent Conducting Films. *Adv. Mater.* **2010**, *22*, 3558–3563.
25. Wu, H.; Kong, D. S.; Ruan, Z. C.; Hsu, P. C.; Wang, S.; Yu, Z. F.; Carney, T. J.; Hu, L. B.; Fan, S. H.; Cui, Y. A Transparent Electrode Based on a Metal Nanotrough Networks. *Nat. Nano.* **2013**, *8*, 421–425.
26. Catrysse, P. B.; Fan, S. Nanopatterned Metallic Films for Use as Transparent Conductive Electrodes in Optoelectronic Devices. *Nano Lett.* **2010**, *10*, 2944–2949.
27. Kim, Y. H.; Sachse, C.; Machala, M. L.; May, C.; Müller-Meskamp, L.; Leo, K. Highly Conductive PEDOT: PSS Electrode with Optimized Solvent and Thermal Post-Treatment for ITO-Free Organic Solar Cells. *Adv. Funct. Mater.* **2011**, *21*, 1076–1081.
28. Carlé, J. E.; Andersen, T. R.; Helgesen, M.; Bundgaard, E.; Jørgensen, M.; Krebs, F. C. A Laboratory Scale Approach to Polymer Solar Cells Using One Coating/Printing Machine, Flexible Substrates, No ITO, No Vacuum and No Spincoating. *Sol. Energy Mater. Sol. C* **2013**, *108*, 126–128.
29. Huang, Y. C.; Hsu, F. H.; Cha, H. C.; Chuang, C. M.; Tsao, C. S.; Chen, C. Y. High-Performance ITO-Free Spray-Processed Polymer Solar Cells with Incorporating Inkjet Printed Grid. *Org. Electron.* **2013**, *14*, 2809–2817.
30. Kang, M. G.; Guo, L. J. Nanoimprinted Semitransparent Metal Electrodes and Their Application in Organic Light-Emitting Diodes. *Adv. Mater.* **2007**, *19*, 1391–1396.
31. Galagan, Y.; Zimmermann, B.; Coenen, E. W. C.; Jørgensen, M.; Tanenbaum, D. M.; Krebs, F. C.; Gorter, H.; Sabik, S.; Slooff, L. H.; Veenstra, S. C.; *et al.* Current Collecting Grids for ITO-Free Solar Cells. *Adv. Energy Mater.* **2012**, *2*, 103–110.
32. Van Osch, T. H.; Perelaer, J.; de Laat, A. W.; Schubert, U. S. Inkjet Printing of Narrow Conductive Tracks on Untreated Polymeric Substrates. *Adv. Mater.* **2008**, *20*, 343–345.
33. Ahn, B. Y.; Duoss, E. B.; Motala, M. J.; Guo, X. Y.; Park, S. I.; Xiong, Y. J.; Yoon, J.; Nuzzo, R. G.; Rogers, J. A.; Lewis, J. A. Omnidirectional Printing of Flexible, Stretchable, and Spanning Silver Microelectrodes. *Science* **2009**, *323*, 1590–1593.
34. Aernouts, T.; Vanlaeke, P.; Geens, W.; Poortmans, J.; Hermans, P.; Borghs, S.; Mertens, R.; Andriessen, R.; Leenders, L. Printable Anodes for Flexible Organic Solar Cell Modules. *Thin Solid Films.* **2004**, *451*, 22–25.
35. Song, T. B.; Chen, Y.; Chung, C. H.; Yang, Y. M.; Bob, B.; Duan, H. S.; Li, G.; Tu, K. N.; Huang, Y.; Yang, Y. Nanoscale Joule Heating and Electromigration Enhanced Ripening of Silver Nanowire Contacts. *ACS Nano* **2014**, *8*, 2804–2811.
36. Reineke, S.; Lindner, F.; Schwartz, G.; Seidler, N.; Walzer, K.; Lussem, B.; Leo, K. White Organic Light-Emitting Diodes with Fluorescent Tube Efficiency. *Nature* **2009**, *459*, 234–238.
37. De, S.; Higgins, T. M.; Lyons, P. E.; Doherty, E. M.; Nirmalraj, P. N.; Blau, W. J.; Boland, J. J.; Coleman, J. N. Silver Nanowire Networks As Flexible, Transparent, Conducting Films: Extremely High DC to Optical Conductivity Ratios. *ACS Nano* **2009**, *3*, 1767–1774.
38. Zou, J.; Yip, H. L.; Hau, S. K.; Jen, A. K.-Y. Metal Grid/Conducting Polymer Hybrid Transparent Electrode for Inverted Polymer Solar Cells. *Appl. Phys. Lett.* **2010**, *96*, 203301.
39. Kang, M. G.; Kim, M. S.; Kim, J.; Guo, L. J. Organic Solar Cells Using Nanoimprinted Transparent Metal Electrodes. *Adv. Mater.* **2008**, *20*, 4408–4413.
40. Villani, F.; Vacca, P.; Nenna, G.; Valentino, O.; Burrasca, G.; Fasolino, T.; Minarini, C.; della Sala, D. Inkjet Printed Polymer Layer on Flexible Substrate for OLED Applications. *J. Phys. Chem. C* **2009**, *113*, 13398–13402.
41. Raut, H. K.; Ganesh, V. A.; Nair, A. S.; Ramakrishna, S. Anti-Reflective Coatings: A Critical, In-Depth Review. *Energy Environ. Sci.* **2011**, *4*, 3779.
42. Lee, C.; Kim, J. J. Enhanced Light Out-Coupling of OLEDs with Low Haze by Inserting Randomly Dispersed Nanopillar Arrays Formed by Lateral Phase Separation of Polymer Blends. *Small* **2013**, *9*, 3858–3863.
43. Adachi, C.; Baldo, M. A.; Thompson, M. E.; Forrest, S. R. Nearly 100% Internal Phosphorescence Efficiency in An Organic Light-Emitting Device. *J. Appl. Phys.* **2001**, *90*, 5048–5051.
44. Gu, G.; Garbuzov, D. Z.; Burrows, P. E.; Venkatesh, S.; Forrest, S. R.; Thompson, M. E. High-External-Quantum-Efficiency Organic Light-Emitting Devices. *Opt. Lett.* **1997**, *22*, 396–398.
45. Bulović, V.; Khalfin, V. B.; Gu, G.; Burrows, P. E.; Garbuzov, D. Z.; Forrest, S. R. Weak Microcavity Effects in Organic Light-Emitting Devices. *Phys. Rev. B* **1998**, *58*, 3730–3740.
46. Zhou, L.; Ou, Q.-D.; Chen, J.-D.; Shen, S.; Tang, J.-X.; Li, Y.-Q.; Lee, S.-T. Light Manipulation for Organic Optoelectronics with Bio-Inspired Moth's Eye Nanostructures. *Sci. Rep.* **2014**, *4*, 4040.
47. Chen, J. D.; Zhou, L.; Ou, Q. D.; Li, Y. Q.; Shen, S.; Lee, S. T.; Tang, J. X. Enhanced Light Harvesting in Organic Solar Cells Featuring a Biomimetic Active Layer and a Self-Cleaning Antireflective Coating. *Adv. Energy Mater.* **2014**, *4*, 1301777.
48. Yang, J. P.; Bao, Q. Y.; Xu, Z. Q.; Li, Y. Q.; Tang, J. X.; Shen, S. Light Out-Coupling Enhancement of Organic Light-Emitting Devices with Microlens Array. *Appl. Phys. Lett.* **2010**, *97*, 223303.
49. Sun, Y.; Forrest, S. R. Enhanced Light Out-Coupling of Organic Light-Emitting Devices Using Embedded Low-Index Grids. *Nat. Photonics* **2008**, *2*, 483–487.
50. Oulton, R. F.; Sorger, V. J.; Genov, D. A.; Pile, D. F. P.; Zhang, X. A Hybrid Plasmonic Waveguide for Subwavelength Confinement and Long-Range Propagation. *Nat. Photonics* **2008**, *2*, 496–500.
51. Zhou, W.; Wu, Y.; Yu, M.; Hao, P.; Liu, G.; Li, K. Extraordinary Optical Absorption Based on Guided-Mode Resonance. *Opt. Lett.* **2013**, *38*, 5393–5396.
52. Jin, Y.; Feng, J.; Zhang, X. L.; Bi, Y. G.; Bai, Y.; Chen, L.; Lan, Liu; T, Y. F.; Chen, Q. D.; Sun, H. B. Solving Efficiency-Stability Tradeoff in Top-Emitting Organic Light-Emitting Devices by Employing Periodically Corrugated Metallic Cathode. *Adv. Mater.* **2012**, *24*, 1187–1191.
53. Bai, Y.; Feng, J.; Liu, Y.-F.; Song, J.-F.; Simonen, J.; Jin, Y.; Chen, Q.-D.; Zi, J.; Sun, H.-B. Outcoupling of Trapped Optical Modes in Organic Light-Emitting Devices with One-Step Fabricated Periodic Corrugation by Laser Ablation. *Org. Electron.* **2011**, *12*, 1927–1935.
54. Christ, A.; Zentgraf, T.; Kuhl, J.; Tikhodeev, S.; Gippius, N.; Giessen, H. Optical Properties of Planar Metallic Photonic Crystal Structures: Experiment and Theory. *Phys. Rev. B* **2004**, *70*, 125113.